Biodegradability, physical, mechanical and antimicrobial attributes of starch nanocomposites containing chitosan nanoparticles

Mehran Babaee[a], Farhad Garavand[b*], Abdur Rehman[c], Shima Jafarazadeh[d], Elahe Amini[e], Ilaria Cacciotti[f*]

[a]Department of Wood and Paper, Faculty of Agriculture and Natural Resources, University of Tehran, Karaj, Iran (mn.babaee@gmail.com)

[b]Department of Food Chemistry and Technology, Teagasc Food Research Centre, Moorepark, Fermoy, Co. Cork, Ireland (farhad.garavand@teagasc.ie)

[c]State Key Laboratory of Food Science and Technology, Jiangnan University, Wuxi, China (hafizje145@gmail.com)

[d]School of Engineering, Edith Cowan University, Joondalup, WA 6027, Australia (shimajafar@yahoo.com)

[e]CELBIOTECH Research Group, School of Industrial, Aerospace and Audiovisual Engineering, Universitat Politècnica de Catalunya, BarcelonaTech, 08222 Terrassa, Spain (elahe.amini@upc.edu)

[f] Department of Engineering, INSTM RU, University of Rome "Niccolò Cusano", Roma, Italy (ilaria.cacciotti@unicusano.it)

*Corresponding authors email addresses: ilaria.cacciotti@unicusano.it (Ilaria Cacciotti) & farhad.garavand@teagasc.ie (Farhad Garavand)

Abstract

This study aimed to develop a plasticized starch (PS) based film loaded with chitosan nanoparticles (CNPs, 1, 2, 3, and 4%) as a reinforcing and antibacterial agent. We examined the morphology, biodegradability, mechanical, thermo-mechanical, and barrier properties of the PS/CNPs films. The antimicrobial activity against both Gram-positive (*S. aureus*) and Gram-negative (*E.coli*) bacteria was investigated by colony forming unit (CFU) and disc diffusion methods. A dense structure was obtained for all PS/CNPs films and, thus, their complete biodegradation occurred in more days than neat PS. The increase in the CNPs percentage led to improved mechanical behaviour and barrier properties. PS-CNPs composite films revealed inhibition zones against both *E.coli* and *S. aureus*, with the 100% reduction in CFU against *S. aureus*. The current study exhibited that PS-CNPs films were more effective in inhibiting bacteria growth than neat PS film, confirming the composite films potential application as antimicrobial food packaging.

Keywords: Starch/chitosan nanocomposites; Antimicrobial activity; Food packaging.

1. Introduction

Increasing demands in terms of ready to eat foods, including sandwiches, mixed salads and fresh-cut fruits, by consumers have forced the food technologists and researchers to find out innovative approaches that can inhibit the microbes' growth and improve the durability of foods [1]. Antimicrobial nanocomposite strategy is an auspicious preservation practice that can hinder the growth of microbes in the food systems, as well as extend the shelf life of foods [2]. Indeed, antimicrobial agents loaded nanocomposite materials could progressively release the antimicrobial agents on the surface of foods in order to improve their shelf life by combating the microbial growth [3]. Biopolymers have successfully been recognized as promising materials for food packaging, because they are completely biodegradable, inexpensive, renewable and globally present in the markets [4-7]. Among them, thermoplastic starch, obtained from native starch with a disruption of its structure and related crystallinity decrease [8], is gaining a lot of interest. Numerous plasticizers, including sorbitol, glycerol, and water, are being used to obtain thermoplastic starch. While comparing with other thermoplastic biopolymers, thermoplastic starch has exhibited two leading drawbacks, i.e. higher water sensibility and weaken mechanical characteristics [9]. In order to beat the aforementioned constraints, the loading of reinforcing agents, including whiskers, nanoparticles, and nanofibers, in the starch matrix offers great avenues to develop starch-based nanocomposites [10-12]. Nevertheless, there are numerous assumptions regarding poisonousness of nanoparticles, that could penetrate into the human tissues, because of their very small diameter (<100 nm), resulting in severe damage to the human skin [13], [14]. On the other hand, nanoparticles fabricated by natural biopolymers, e.g. cellulose, chitosan, pectin, alginate, have been widely used as nanofillers [15], and are commonly recognized as safe and edible without any side effect. Amongst them, chitosan nanoparticles (CNPs), derived from crab or shrimp shells and fungal mycelia, have recently gained more popularity as a substitute to micro-sized

reinforcements in biocomposite materials [9], and have successfully been used in water treatment, textile industry, food coating, food packaging and nanocomposites [5], [16], [17]. Moreover, recent investigations have proposed that incorporation of CNPs into the biopolymers can provide antimicrobial functionalities, since chitosan display virtuous antimicrobial properties. For example, a recent work by Vahedikia and co-workers reported that loading of 4% CNPs into biodegradable zein films significantly contributed to the tensile strength enhancement, associated to a decreased elongation, and allowed to induce an inhibitory zone particularly against *Escherichia coli* (*E. coli*) and *Staphylococcus aureus* (*S. aureus*) [18]. Similarly, in another study, the influence of CNPs coating was examined on the microbiological property of fresh-cut apple slices. It was reported that CNPs coating could constrain growth of yeasts, molds, psychotropics, yeasts, and mesophilic bacteria on apple slices consequently naked out the strong usage of CNPs in antimicrobial composites [19]. Therefore, CNPs could be proposed as potent nanofillers for development of reinforced antimicrobial nanocomposites.

In this framework, the aim of the present study was to evaluate the influence of CNPs loading on the physico-mechanical, biodegradation and antimicrobial properties of the starch-based nanocomposites.

2. Materials and methods

2.1. Materials

Chitosan (low molecular weight) and corn starch (5% amylose and 65% amylopectin) were purchased from Sigma-Aldrich, USA and Alborz Starch Co., Iran, respectively. Acetic acid, glycerol, methanol, acetone, methacrylic acid and malt extract agar (MEA) were supplied by Merck Chemical Co. (Darmstadt, Germany) and Minatajhiz Co. (Tehran, Iran). The stock culture of white rots fungus (*Trametes versicolor*), used as selected fungus, as well as *E. coli* and *S. aureus* were provided by the National Collection of Biology Laboratory, University of Tehran (Tehran, Iran). Brain heart infusion (BHI), tryptic soy (TS), and Luria–Bertani (LB) media were supplied by Difco (Detroit, USA).

2.2. Preparation of CNPs

CNPs were engineered by means of ionotropic gelation of chitosan (1% (w/v)), using sodium tripolyphosphate (1% (w/v)) [20], with little adjustments. In this regard, chitosan solution was prepared, using 2% (v/v) acetic acid. Subsequently, 8 mL of TPP aqueous solution was added dropwise (rate of 1 ml/min) into 200 ml of chitosan solution under continuous magnetic stirring at room temperature. The prepared mixture was maintained on stirrer for 30 min, submitted to sonication for 30 min, and, finally, centrifuged at 12,000 rpm for 20 min. The obtained precipitates were washed with water, centrifuged again twice, washed with ethanol, and subsequently dried out.

2.3. Preparation of CNPs-loaded plasticized starch-based nanocomposite

CNPs suspension was prepared by ultrasonication in a solution of refined water (100 ml) and glycerol (1.5 g) for 30 min. Then 5 g corn starch were added. The various concentrations of CNPs (1, 2, 3 and 4 wt. %) were related to the starch amount. The mixtures were heated at 90 °C for 30 min under continuous stirring to induce starch plasticization. For the production of PS-CNPs composite films, the mixtures were cast into Petri dishes and dried at 50 °C about 6

h, in an oven. The obtained samples were preconditioned at 25 °C and 50% RH, in a climate chamber, for at least 48 h prior to the characterisation. The films water content was around 10 wt. %, determined by standard oven drying method.

2.4. Characterization of CNPs

2.4.1. Atomic force microscopy

Atomic force microscopy (AFM) was employed to investigate the size distribution and morphological characterization of CNPs-PS suspensions. A drop (0.05 mg/ml) of diluted CNPs-loaded nanocomposite suspension was placed on the clean glass surface, and kept at 25 °C for drying. All images were acquired in tapping mode using resonance frequency of 150–190 kHz, silicon probe cantilever of 230 micron length, spring constant of 20–60 N/m, tip radius of curvature of 5–10 nm, scanning rate of 1 Hz.

2.4.2. Particle size distribution

The CNPs size distribution within the nanocomposite suspensions was measured through a Zetasizer Nano ZS 3300 (Malvern Instruments Ltd., United Kingdom), based on the dynamic light scattering phenomenon. All samples were diluted 100 times, and the diluitions were filled inside the glass cuvette with square aperture, and then scattering intensity was detected at 25 °C.

2.5. Characterization of CNPs-loaded PS films

2.5.1. Physical properties

Water absorption (WA) analysis was carried out using ASTM standard E104. For water absorption test, samples with dimensions of 2×2 cm^2 were separated from PS, PS-1CNPs, PS-2CNPs, PS-3CNPs, and PS-4CNPs composites, further dried at 60 °C for 24 h, and kept inside the desiccator comprising calcium sulphate (RH = 0%) for 3 days. Subsequently, the initial samples weight was recorded. Then, all samples were put into a desiccator encompassing

potassium sulfate (RH = 98%), and time required to achieve a constant weight was detected. Finally, WA of all samples was measured by the following equation (Eq. 1).

$$WA = \frac{W1-W0}{W0} \times 100 \quad (1)$$

where W_1 and W_0 are the sample weight the after exposure to 98% RH and the initial sample weight, respectively. All tests were carried out in triplicates to provide mean values.

Water vapor transmission rate (WVTR) tests were carried out gravimetrically by adopting the ASTM standard E 96 (1996) [21], with little adjustments. All samples were stored inside the chamber comprising calcium sulfate in order to offer a constant 50% RH at 25 °C for 24 h. At that point, all samples were organized on glass cups holding calcium sulfate (3 g), which delivers 0 % RH. Firstly, the cup assemblies were weighed out by electronic balance and transferred into a desiccator having controlled temperature zone (25 ± 0.5 ° C) and RH (98 ± 2%). Weight changes in function of time were recorded. A simple linear regression method was employed to determine the slope of the linear portion.

WVTR was measured by using Eq. 2:

$$WVTR = \frac{\frac{G}{t}}{A} = \frac{Slope}{Test\ area} \quad (2)$$

where G, t, A, G/t are the changes in the weight (g), the time (h), the area exposed to moisture transfer (m^2), the slope attained from a chart between changes in weight and time, respectively. Linear regression of complete information presented a correlation coefficient >95%.

Water vapor permeability (WVP) was evaluated by using Eq. 3:

$$WVP = \frac{WVTR}{P \times (R1-R2)} \times X \quad (3)$$

where P, X, R_1 and R_2 are the saturation water vapor pressure at 25 °C (Pa), the film thickness (m), the RH in the desiccator (98% RH), and the RH in the cups (0% RH), respectively.

2.5.2. Mechanical testing

ASTM standard (D889) was adopted to investigate the mechanical properties of composites. Before examining, all samples (70×10 mm^2) were stored in a desiccator at room temperature and 55% RH for a week. The tensile tests were performed with an Instron mechanical machine (M350-10-CT) equipped with a crosshead speed of 4 mm/min, gauge length of 50 mm, and a 500 N load cell. The elastic modulus was determined through initial slope of the tensile curves. For each composite kind, five samples were analyzed and the mean values and related standard deviations are presented.

2.5.3. Dynamic mechanical thermal analysis (DMTA)

PS-CNPs dynamic mechanical thermal behaviour was investigated from -50 to 150 °C (heating rate of 2 °C/min), employing a Mark Netzsch DMA242 analyzer, operating at 3.33 Hz frequency in tensile mode. All films were cut into rectangular samples (approximately 20.0 × 5.0 × 0.6 mm^3), and the tests were performed in triplicate in order to provide average values and related standard deviation.

2.5.4. Biodegradation analysis

The composites biodegradation analysis was performed, using a white rot fungus (i.e. *Tinea versicolor*) and samples with cross dimensions of 20.0 × 10.0 × 0.4 mm^3 (length × width × thickness). Afterwards, they were put into an oven at 70 °C overnight and, primary weight of each sample was documented. The filtered fungus was poured into the Petri dishes comprising MEA, and Petri dishes were incubated at 25 °C and 90% HR for 24 h in order to completely cover culture medium by the fungus, after that, all samples were transferred into the Petri dishes comprising culture medium. In order to avoid direct contact with culture medium, all samples were mounted over 2 mm stages. All Petri dishes encompassing all samples and the fungus medium were kept inside the incubator operating at 25 °C and 75% RH. The rate of biodegradation for all samples was assessed by

weight difference before and after exposure of all samples to the white rot fungus for 2 months, with regular intervals of 10 days.

The rate of fungus degradation was measured by following Eq. (4).

$$DE = \frac{W0-W1}{W0} \times 100 \quad (4)$$

where DE, W_0, W_1 are the biodegradation rate (%) of the film, the initial sample weight, and the dry weight of the residual sample after exposure to the white rot fungi for a specific time, respectively.

2.5.5. Scanning electron microscopy (SEM)

The cross-sectional and surface appearance of all composites were inspected before and after degradation phenomenon through a SEM, model ZEISS Ultra 55, Germany. After biodegradation tests at 25 °C, all samples were separated from the culture medium, and cautiously cleaned by purified water in order to eradicate the fungal mycelium. Before the SEM observation, all samples were sputter coated with gold for 30 s under vacuum (10^{-2} Torr). The operating acceleration voltage was fixed at about 10 kV.

2.5.6. Antimicrobial properties

2.5.6.1. Colony forming count method

The produced composites antimicrobial behaviour was investigated by means of the colony forming count method as reported by Rhim et al. [22]. Two microorganisms, i.e. *E. coli* and *S. aureus*, were used as Gram-positive (G-positive) bacteria and Gram-negative (G-negative) bacteria, respectively. Briefly, square specimens (10×10 cm^2) were inserted in sterile flasks. *S. aureus* and *E. coli* strains were cultured, under aerobic conditions for 24 h, in TS broth at 30 °C and BHI broth at 37 °C, and, respectively. The prepared inocula (100 mL per each) were diluted 10 times in broth and then aseptically transferred to the flasks comprising the PS composite films to obtain a concentration ca. 2.0×10^6 CFU/mL. A bacterial cells inoculum in a flask without composite films was considered as control. The flasks were placed in a shaker

incubator (S-150 Model, Stuart, UK) at 100 rpm and 30 ° C. Samples were periodically taken and plated on the BHI and TS agar media for G-positive and G-negative bacteria, respectively, and then incubated for 48 h at 37 ° C and 30 °C for BHI agar and TS agar, respectively. Every test was conducted in triplicates and the data stated as the mean CFU/mL.

2.5.6.2. Disc diffusion method

This test was performed according to Dehnad et al. [23] with slight modifications. A loop of each bacterium (*E. coli* and *S. aureus*) was inoculated in 50 mL LB sterile medium. Then the cultured bacterial strains (in LB) were agitated at 200 rpm for 24 h at 37 ° C in a shaker incubator (S-150 Model, Stuart, UK). Various dilution series of bacterial populations were prepared using peptone water. The plasticized starch films reinforced with CNPs were cut into disc shape samples (diameter of 1.5 cm), placed on LB agar plates, and incubated at 37 °C for 24 h. The antimicrobial activity was qualitatively evaluated on the basis of the diameter of the inhibitory zone nearby the contact area of the film with agar surface. Agar plates were earlier seeded with 0.1 mL (equal to about 10^6 CFU/mL of bacterial strains) overnight, and the strains were incubated at 37 °C for 24 h.

2.6. Statistical analysis

The obtained data were subjected to one way analysis of variance (ANOVA) and the significance differences between the means of groups were compared by Duncan's multiple range test at significance level of 0.05 using SPSS software (V23, SPSS Inc., USA).

3. Results and discussion

3.1. Characterization of CNPs

AFM imaging is being used as an efficacious approach to investigate the size distribution and surface morphology of nanoparticles. AFM images established the nanosized and spherical structure of CNPs, as shown in Fig. 1a. The size distribution directed that most of CNPs were

found in the range of 28.5-51.4 nm (Fig. 1a). Though, CNPs size observed in this study is smaller as compared to previous works, very probably due to the different chitosan and TPP concentrations, even if the same procedure was followed, as evidenced by Calvo and his co-authors [24]. For instance, de Moura et al. declared a particles size in the range of 85-221 nm, stating that lowest concentration of TPP and chitosan offered minor droplets size [25]; Chang and co-workers reported a 50-100 nm range for the particle size distribution in the case of CNPs fabricated by using 1% (w/v) chitosan and TPP [26].

Dynamic light scattering approach was exploited to explore the particle size distribution and mean particle size of fabricated CNPs. Fig. 1b confirms a particle size distribution profile for all kinds of CNPs with a diameter range between 7.3 nm and 125.17 nm, proposing a fine size distribution (polydispersity index <1). It has been reported that nanoparticles size measured in hydrated state was higher to some extent as compared to the nanoparticles size observed in dried state [27].

3.2. Characterization of composite films

3.2.1. Physical properties

The water absorption of the neat PS and composites entrapped with CNPs was examined at a 98% RH. In the initial step, an increasing trend in the moisture absorption of the neat PS and CNPs-loaded composites was reported; whereas, a plateau trend in water uptake was observed at the final hours of the experiments (Fig. 2). Furthermore, the water uptake of PS-1CNPs, PS-2CNPs, PS-3CNPs, and PS-4CNPs composites was significantly lower with respect to neat PS, and it progressively decreased increasing the CNPs concentration. The minimum reduction was observed for PS-4CNPs composite as compared to other composites. Comparable findings were also reported by Hietala et al. [10], ascribing them to branch and amorphous structure of starch.

In order to reduce the influence of water vapor, starch-based composites should prevent, or at least be able to minimize the moisture level, moisture transfer with the surroundings, meaning that WVP should be minimized as much as possible. The WVP and WVTR values of PS and PS-CNPs films were determined and related data are collected in Table 1, indicating that water vapor easily permeated all the PS based samples. The neat PS film exhibited the highest WVP and WVTR values, whereas a progressively declining trend in WVP and WVTR values was observed when 1-4 wt.% CNPs were added to the PS matrix. Similar findings were previously observed for sago starch plasticized with glycerol [28]. The loading of CNPs into the polymeric-based matrixes probably led to the obtainment of denser and less permeable structures. In addition, an efficient interfacial adhesion and compatibility between the starch matrix and CNPs might be a leading reason to confine the moisture diffusion rate.

3.2.2. Mechanical properties

Table 2 collects the mechanical properties of all fabricated composites, in order to evidence the CNPs influence

on the mechanical behaviour of the produced films. As nanofillers inside the starch-based composites, CNPs exhibited an apparent enforcement influence. A significant and progressive improvement of the tensile strength (TS) and the Young's modulus (E) values of all composites by increasing the CNPs concentration was revealed, whereas a declining trend in terms of elongation at break (EAB), as expected. In details, a remarkable increment in tensile strength from 9.54 to 24.91 MPa and in Young's modulus from 16.50 MPa to 47.11 MPa was detected varying the CNPs content from 0 to 4 wt.%, while the elongation at break declined from 51.01% to 34.29%. These experimental evidences might be ascribed to the good interphase between CNPs and PS, owing to the identical polymeric structures of starch and chitosan, to the development of hydrogen bonding arrangement and also to the entanglement of nanofillers

[29]. Furthermore, the establishment of hydrogen bonding can produce a sturdy boundary among two phases including matrixes and nanofillers [30]. Thus, CNPs acted as an effective reinforcing agent, increasing the tensile strength and decreasing the elasticity of PS films.

3.2.3. Dynamic mechanical thermal properties

DMTA is the most suitable characterisation technique to estimate the enhancement in stiffness of composite materials, due to the encapsulation of nanofillers [31]. Fig. 3 represents the storage modulus (E') and the tan δ *vs* the temperature of the produced composites. It is well known that usually the storage modulus reduces by increasing the temperature [32], as presented in Table 3, which collects the E' values for all prepared films at two diverse temperatures, i.e. 25 °C and 70 °C. Fig. 3a depicts that the storage modulus (E') of PS-CNPs composites improved by loading CNPs nanofillers. Such enhancement was more expected because of strong and good interaction between CNPs and PS matrixes [21]. E' results of the PS-CNPs composites at room temperature were in accordance with findings obtained from tensile analysis (Table 2). All composites storage modulus comprising 1-4 wt% CNPs at 25 °C increased to 1258, 1520, 1740, and 1810 MPa, respectively, whereas neat PS presented the lowest value, i.e. 462 MPa. This result might be attributed to the production of an arrangement of CNPs after vaporization of water as well as the development of satisfactory cross-linkages between the matrixes phases in the produced composites [33], [34]. Similarly, it is expected that the CNPs nanofillers constrained the movements of molecular chains of the PS, thus enlightening its thermal stability [35]. Fig. 3b illustrates how CNPs nanofillers can impact on the tan δ at the topmost point of the curve. The changes in the tan δ of PS-based films fortified with nanofillers were hardly to evaluate, for that reason tan δ was not properly precise. However, the DMTA analysis were investigated in triplicate in order to make sure the data accuracy, and similar curves were obtained in all cases, in agreement with a study on potato

starch films [36]. Table 3 highlights the tan δ peak temperature values, correspondent to the material glass transition temperature (T_g), designed for all produced PS and PS/CNPs films. The peak site for the PS happened at 46 °C, and improved to 77, 83, 101 and 103°C for CNPs-loaded PS-composites. This increment in values of tan δ by means of temperature specifies that the produced composites could become more viscous after rising the temperature. This improvement in storage modulus as well as the tan δ peak shift for PS-CNPs composites might be because of the potent interaction among polymeric matrixes and nanofillers, that have the ability to restrict the polymeric chains segmental mobility in the neighbourhood of the nanofillers [37]. In conclusion, our findings approved that the CNPs addition to the PS matrix allowed to significantly improve the polymer dynamic mechanical properties.

3.2.4. Biodegradability of PS and PS-CNPs films

The PS and PS-CNPs films biodegradability was examined using white rot fungi (*T. versicolor*) and calculating the loss in weight at regular intervals of time. Fig. 4a displays the loss in weight in function of the elapsed time during the degradation process. As a result of rising the decomposition time, the films firmness decreased. All films exhibited a fast degradation process during storage of first 30 days. After 20 days, almost 50 wt % loss in weight of the total solids was detected for all samples. Our findings depicted that PS completely degraded in 40-50 days of storage, whereas fully degradation of the CNPs-loaded composites occurred in 50-60 days. Thus, the addition of CNPs allowed providing a superior resistance in response to degradation in comparison with neat PS. This could be accredited to the denser assembly and crystallinity property of CNPs that was entrapped inside the starch matrixes, in order to restrict the damaging enzymatic performances [38]. It has to be taken into account that numerous factors, such as a wide range of microbes and their existence, the accessibility of carbon-based

sources, and time duration of the observation period, can affect the degradation phenomenon of PS [39].

The microbes have a potent potential in the existence of carbon/hydrogen groups. In terms of PS-CNPs, the substitution groups of CNPs with the hydroxyl groups while modification led to the significant reduction in the rate of decomposition as well as the microbes action [40]. Fig.4b presents the visual aspect of PS and PS-CNPs films exposed to the white rot fungi up to 40 days for neat PS and 60 days for composite films, at intervals of 10 days. It was concluded that all samples significantly eroded: the original shape of all samples was lost by over time and it can be clearly perceived that samples color changed from yellow to dark brown. However, this process was faster in the case of neat PS. Thus, our findings obviously proved that the CNPs can enhance the degradation span of all produced composites with respect to neat PS.

3.2.5. Morphology of composites

The possible variations occurred in the structure and morphology of composites were successfully investigated before and after treatment with fungi. SEM micrographs of the neat PS and PS-CNPs surfaces are presented in Fig. 5. Neat PS film exhibited smooth surface as compared to other composites, with exceptional structure integrity (Fig. 5A). Diverse changes in structure of composites surface were reported after encapsulation of CNPs into the PS-based composites. PS-1CNPs film was characterised by a very homogeneous and uniform CNPs dispersion within the polymeric matrix, without noticeable aggregation (Fig. 5B), whereas the presence of small aggregates could be evidenced for PS-2CNPs (Fig. 5C), and PS-3CNPs (Fig. 5D) samples. Moreover, whereas the agglomeration of CNPs was clearly observed at the highest nanofiller content (4%, w/w) (Fig. 5D). However, a dense morphological structure was observed by loading of different concentrations of CNPs as compared to the pure PS. This enlightened through the amended barrier and mechanical properties of produced composites

because of excellent bonding network among polymer and nanofillers. Our results are correlated with the findings of Chang et al. [26], who studied on starch-based composites loaded with nanoparticles. Fig. 5 points out the clear SEM results of the PS and the PS-CNPs composites after exposure to the fungus medium for 30 days of storage, wherein a clearance development of fungal and mycelium rudiments could be seen on the samples. After exposure to the fungus medium, all composites gained rough structure, as well as a decrease in the thickness. The results predicted that the therapeutic effect of fungi decreased by varying the surface of nanofillers from hydrophilic to hydrophobic.

3.2.6. Antimicrobial properties

The antimicrobial activities of the neat PS film and of its composites, i.e. PS-1CNPs, PS-2CNPs, PS-3CNPs, and PS-4CNPs were analyzed against *E.coli* and *S. aureus* by MEANS OF agar disc diffusion and the colony-forming count methods. The results of the agar disc diffusion method for PS film and its composites with 1, 2, 3 and 4% CNPs are shown in Fig. 6a-d and Fig. 7a-d. As evident, no inhibition zone against *E. coli* or *S. aureus* was revealed in the case of the control PS film (without CNPs) (Fig. 6 and Fig. 7), therefore presenting no antibacterial activity, as expected [41-43]. On the contrary, the incorporation of CNPs in PS film resulted in the inhibitory zones against both G-negative and G-positive bacteria, as evident in Fig. 6a-d and Fig. 7a-d. The results also demonstrated that the CNPs concentration increment from 0% to 4% in PS film led to a progressively higher antibacterial activity against both G-negative and G-positive bacteria, as testified by the progressively larger inhibition zone area. This could be due to the effective antimicrobial activity of the CNPs [44], in agreement with Ali et al. [45] who claimed the increased concentration of CNPs from 0.01% to 0.04% in polyethylene terephthalate film led to increasing the antimicrobial activity against *S. aureus*. Moreover, comparing Fig. 6 and Fig. 7, it is evident that CNPs were more efficient in inhibiting G-positive

bacteria than G-negative bacteria, and *S. aureus* was more susceptible to CNPs than *E.coli*. This finding is similar with results by Antoniou et al. [16] who stated that G-negative bacteria were more resistant to the CNPs than G-positive bacteria. Moreover, Hosseini et al. [46] reported that the gelatin film loaded with CNPs did not show inhibition zone on G-negative bacteria (*E.coli*). This attribute could be due to the fact that the negative gram bacteria present a composite cell wall structure with thin peptidoglycan layer banded by an outer membrane; therefore, the CNPs initially attach to the outer cell membrane of bacteria, which includes phospholipids, lipopolysaccharide, and lipoprotein, reducing their adhesion. On the contrary, the G-positive bacteria own a thick cell wall structure with peptidoglycan multilayers, and, thus, the CNPs could immediately connect to their outer cell wall, equipped of many pores to allow CNPs quick penetration into the cells. Thus, the CNPs could be able to disrupt the cytoplasmic membrane, causing the intracellular content leakage and cell death [47]. Additionally, Shapi'i et al. [43] stated that the non-volatile character of CNPs could limit the effectiveness of their antimicrobial activity against gram-negative bacteria.

Additionally, the antimicrobial behaviour of PS, PS-1CNPs, PS-2CNPs, PS-3CNPs, and PS-4CNPs samples was also examined by applying the CFU counting to confirm the findings obtained with the disc diffusion method. The results of the CFU method for PS film and its composites against *E.coli* and *S. aureus* are reported in Table 4a-d. The findings showed that the control PS film (without CNPs) did not own antimicrobial activity, and the number of colonies increased for both *E.coli* and *S. aureus* under all concentrations during contact time. On the contrary, the inhibitory action of PS-CNPs films progressively enhanced with increasing the CNPs concentration from 1% to 4%, leading to a greater antimicrobial effect. On average a reduction in CFU of 53.16%, 68.02%, 77.60% and 81.77% for *E.coli* was obtained in presence of PS-1CNPs, PS-2CNPs, PS-3CNPs, and PS-4CNPs respectively. Moreover, a much higher reduction in the CFU for *S. aureus* was revealed for all CNPs concentrations. The results

showed that the PS-CNPs films in all concentrations (1%-4%) provided full reduction (100%) for *S. aureus*, displaying that PS-CNPs films were more effective in inhibiting G-positive bacteria growth than that of G-negative bacteria, and, thus, confirming the disc diffusion method findings.

Conclusions

Neat PS film and PS-CNPs films were successfully prepared, incorporating within PS matrix synthesised CNPs in different concentrations (1%-4%) as a reinforcing agent and an active antimicrobial agent. Neat PS film exhibited smooth surface, while PS-CNPs composites presented rougher surface and the presence of CNPS agglomerates increasing the nanofiller content (4%, w/w). The tensile strength, Young's modulus, WVP, and water uptake of films were improved with an increase in CNPs. Moreover, the antibacterial action was demonstrated, and biodegrading duration of bio-composites moderately increased with respect to thermoplastic starch composite. PS-CNPs films showed excellent antimicrobial properties against both G-negative and G-positive bacteria, resulting more effective in inhibiting G-positive bacteria growth; besides, the antimicrobial impact progressively enhanced with increasing the CNPs concentration. Overall, this study suggests that CNPs loaded PS films own excellent potential to be exploited as active food packaging.

References

[1] R. Bahrami, R. Zibaei, Z. Hashami, S. Hasanvand, F. Garavand, M. Rouhi,. . . R. Mohammadi, Modification and improvement of biodegradable packaging films by cold plasma: a critical review, Critical reviews in food science and nutrition (2020) 1-15.

[2] I. Solaberrieta, A. Jiménez, I. Cacciotti, M. C. Garrigós, Encapsulation of bioactive compounds from aloe vera agrowastes in electrospun poly (ethylene oxide) nanofibers, *Polymers* 12(6) (2020) 1323.

[3] L. Motelica, D. Ficai, A. Ficai, O. C. Oprea, D. A. Kaya, E. Andronescu, Biodegradable antimicrobial food packaging: Trends and perspectives, *Foods 9*(10) (2020) 1438.

[4] F. Garavand, M. Rouhi, S. H. Razavi, I. Cacciotti, R. Mohammadi, Improving the integrity of natural biopolymer films used in food packaging by crosslinking approach: A review, *International journal of biological macromolecules 104 (*2017) 687-707.

[5] A. Rehman, S. M. Jafari, R. M. Aadil, E. Assadpour, M. A. Randhawa, S. Mahmood, Development of active food packaging via incorporation of biopolymeric nanocarriers containing essential oils, *Trends in Food Science & Technology 101* (2020) *106-121.*

[6] I. Cacciotti, S. Mori, V. Cherubini, F. Nanni, Eco-sustainable systems based on poly (lactic acid), diatomite and coffee grounds extract for food packaging, *International journal of biological macromolecules* 112 (2018) 567-575.

[7] I. Cacciotti, F. Nanni, Poly(lactic) acid fibers loaded with mesoporous silica for potential applications in the active food packaging, AIP (American Institute of Physiscs) Conference Proceedings 1738 (2016) 270018 (1-4).

[8] P. Balakrishnan, M. Sreekala, M. Kunaver, M. Huskić, S. Thomas, Morphology, transport characteristics and viscoelastic polymer chain confinement in nanocomposites based on thermoplastic potato starch and cellulose nanofibers from pineapple leaf, *Carbohydrate polymers 169* (2017) 176-188.

[9] F. Garavand, I. Cacciotti, N. Vahedikia, A. R. Salara, Ö., Tarhan, S. Akbari-Alavijeh,. . . S. Jafarzadeh, A comprehensive review on the nanocomposites loaded with chitosan nanoparticles for food packaging, *Critical Reviews in Food Science and Nutrition* (2020) 1-34.

[10] M. Hietala, A. P. Mathew, K. Oksman, Bionanocomposites of thermoplastic starch and cellulose nanofibers manufactured using twin-screw extrusion, *European Polymer Journal 49*(4) (2013) 950-956.

[11] A. Mirzaei-Mohkam, F. Garavand, D. Dehnad, J. Keramat, A. Nasirpour, Physical, mechanical, thermal and structural characteristics of nanoencapsulated vitamin E loaded carboxymethyl cellulose films, *Progress in Organic Coatings 138* (2020) 105383.

[12] Y. Zhang, C. Rempel, Q. Liu, Thermoplastic starch processing and characteristics—a review, *Critical Reviews in Food Science and Nutrition 54*(10) (2014) 1353-1370.

[13] A. Mirzaei-Mohkam, F. Garavand, D. Dehnad, J. Keramat, A. Nasirpour, Optimisation, antioxidant attributes, stability and release behaviour of carboxymethyl cellulose films incorporated with nanoencapsulated vitamin E, *Progress in Organic Coatings 134*(2019) 333-341.

[14] A. Rehman, Q. Tong, S. M. Jafari, E. Assadpour, Q. Shehzad, R. M. Aadil,. . . W. Ashraf, Carotenoid-loaded nanocarriers: A comprehensive review, *Advances in colloid and interface science 275* (2020) 102048.

[15] A. Rehman, S. M. Jafari, Q. Tong, T. Riaz, E. Assadpour, R. M. Aadil,. . . A. Ali, Drug nanodelivery systems based on natural polysaccharides against different diseases, *Advances in colloid and interface science* (2020) 102251.

[16] J. Antoniou, F. Liu, H. Majeed, F. Zhong, Characterization of tara gum edible films incorporated with bulk chitosan and chitosan nanoparticles: A comparative study, *Food Hydrocolloids 44*(2015) 309-319.

[17] M. Sivakami, T. Gomathi, J. Venkatesan, H.-S. Jeong, S.-K. Kim, P. Sudha, Preparation and characterization of nano chitosan for treatment wastewaters, *International journal of biological macromolecules 57* (2013) 204-212.

[18] N. Vahedikia, F. Garavand, B. Tajeddin, I. Cacciotti, S. M. Jafari, T. Omidi, Z. Zahedi, Biodegradable zein film composites reinforced with chitosan nanoparticles and cinnamon essential oil: Physical, mechanical, structural and antimicrobial attributes, *Colloids and Surfaces B: Biointerfaces 177* (2019) 25-32.

[19] L. Pilon, P. C. Spricigo, M. Miranda, M. R. de Moura, O. B. G. Assis, L. H. C. Mattoso, M. D. Ferreira, Chitosan nanoparticle coatings reduce microbial growth on fresh- cut apples while not affecting quality attributes, *International Journal of Food Science & Technology 50*(2) (2015) 440-448.

[20] M. L. Tsai, S. W. Bai, R. H. Chen, Cavitation effects versus stretch effects resulted in different size and polydispersity of ionotropic gelation chitosan–sodium tripolyphosphate nanoparticle. *Carbohydrate polymers*, *71*(3) (2008) 448-457.

[21] J. Yu, N. Wang, X. Ma, Fabrication and characterization of poly (lactic acid)/acetyl tributyl citrate/carbon black as conductive polymer composites, *Biomacromolecules 9*(3) (2008) 1050-1057.

[22] J.-W. Rhim, S.-I. Hong, C.-S. Ha, Tensile, water vapor barrier and antimicrobial properties of PLA/nanoclay composite films, *LWT-Food Science and Technology 42*(2) (2009) 612-617.

[23] D. Dehnad, H. Mirzaei, Z. Emam-Djomeh, S.-M. Jafari, S. Dadashi, Thermal and antimicrobial properties of chitosan–nanocellulose films for extending shelf life of ground meat, *Carbohydrate polymers 109* (2014) 148-154.

[24] P. Calvo, C. Remunan- Lopez, J. L. Vila- Jato, M. Alonso, Novel hydrophilic chitosan- polyethylene oxide nanoparticles as protein carriers, *Journal of Applied Polymer Science 63*(1) (1997) 125-132.

[25] M. R. de Moura, F. A. Aouada, R. J. Avena-Bustillos, T. H. McHugh, J. M. Krochta, L. H. Mattoso, Improved barrier and mechanical properties of novel hydroxypropyl methylcellulose edible films with chitosan/tripolyphosphate nanoparticles, *Journal of Food Engineering 92*(4) (2009) 448-453.

[26] P. R. Chang, R. Jian, J. Yu, X. Ma, Fabrication and characterisation of chitosan nanoparticles/plasticised-starch composites, *Food Chemistry 120*(3) (2010) 736-740.

[27] R. Yoksan, J. Jirawutthiwongchai, K. Arpo, Encapsulation of ascorbyl palmitate in chitosan nanoparticles by oil-in-water emulsion and ionic gelation processes, *Colloids and Surfaces B: Biointerfaces 76*(1) (2010) 292-297.

[28] S. Bajpai, C. Navin, L. Ruchi, Water vapor permeation and antimicrobial properties of sago starch based films formed via microwave irradiation, *International Food Research Journal 18*(1) (2011).

[29] M. N. Angles, A. Dufresne, Plasticized starch/tunicin whiskers nanocomposite materials. 2. Mechanical behavior, *Macromolecules 34*(9) (2001) 2921-2931.

[30] M. Sreekala, K. Goda, P. Devi, Sorption characteristics of water, oil and diesel in cellulose nanofiber reinforced corn starch resin/ramie fabric composites, *Composite Interfaces 15*(2-3) (2008) 281-299.

[31] I. Cacciotti, E. Fortunati, D. Puglia, J. M. Kenny, F.Nanni, Effect of silver nanoparticles and cellulose nanocrystals on electrospun poly(lactic) acid mats: morphology, thermal properties and mechanical behaviour, Carbohydrate Polymers 103 (2014) 22– 31.

[32] N. Soykeabkaew, N. Laosat, A. Ngaokla, N. Yodsuwan, T. Tunkasiri, Reinforcing potential of micro-and nano-sized fibers in the starch-based biocomposites, *Composites Science and Technology 72*(7) (2012) 845-852.

[33] A. Mohsin, W. Q. Zaman, M. Guo, W. Ahmed, I. M. Khan, S. Niazi,. . . Y. Zhuang, Xanthan-Curdlan nexus for synthesizing edible food packaging films, *International journal of biological macromolecules* 162 (2020) 43-49

[34] A. J. Svagan, M. A. Azizi Samir, L. A. Berglund, Biomimetic polysaccharide nanocomposites of high cellulose content and high toughness, *Biomacromolecules 8*(8) (2007) 2556-2563.

[35] L. Petersson, K. Oksman, Biopolymer based nanocomposites: comparing layered silicates and microcrystalline cellulose as nanoreinforcement, *Composites Science and Technology 66*(13) (2006) 2187-2196.

[36] Y.-g. Zhou, L.-j. Wang, D. Li, P.-y. Yan, Y. Li, J. Shi,. . . Z.-h. Mao, Effect of sucrose on dynamic mechanical characteristics of maize and potato starch films, *Carbohydrate polymers 76*(2) (2009) 239-243.

[37] D. Bondeson, P. Syre, K. O. Niska, All cellulose nanocomposites produced by extrusion, *Journal of Biobased Materials and Bioenergy 1*(3) (2007) 367-371.

[38] A. Dufresne, J. Castaño, Polysaccharide nanomaterial reinforced starch nanocomposites: A review, *Starch-Stärke 69*(1-2) (2017) 1500307.

[39] M. M. Rashed, A. D. Ghaleb, J. Li, S. A. Al-Hashedi, A. Rehman, Functional-characteristics of Zanthoxylum schinifolium (Siebold & Zucc.) essential oil nanoparticles, *Industrial Crops and Products 161 (2021)* 113192.

[40] W. G. Glasser, B. K. McCartney, G. Samaranayake, Cellulose derivatives with a low degree of substitution. 3. The biodegradability of cellulose esters using a simple enzyme assay, *Biotechnology progress 10*(2) (1994) 214-219.

[41] E. Butnaru, E. Stoleru, M. A. Brebu, R. N. Darie-Nita, A. Bargan, C. Vasile, Chitosan-based bionanocomposite films prepared by emulsion technique for food preservation, *Materials 12*(3) (2019) 373.

[42] D. Kowalczyk, M. Kordowska-Wiater, J. Nowak, B. Baraniak, Characterization of films based on chitosan lactate and its blends with oxidized starch and gelatin, *International journal of biological macromolecules 77* (2015) 350-359.

[43] R. A. Shapi'i, S. H. Othman, N. Nordin, R. K. Basha, M. N. Naim, Antimicrobial properties of starch films incorporated with chitosan nanoparticles: In vitro and in vivo evaluation, *Carbohydrate polymers 230* (2020) 115602.

[44] S. Jafarzadeh, F. Ariffin, S. Mahmud, A. K. Alias, A. Najafi, M. Ahmad, Characterization of semolina biopolymer films enriched with zinc oxide nano rods, *Italian Journal of Food Science 29*(2) (2017).

[45] S. W. Ali, S. Rajendran, M. Joshi, Synthesis and characterization of chitosan and silver loaded chitosan nanoparticles for bioactive polyester, *Carbohydrate polymers 83*(2) (2011) 438-446.

[46] S. F. Hosseini, M. Rezaei, M. Zandi, F Farahmandghavi, Development of bioactive fish gelatin/chitosan nanoparticles composite films with antimicrobial properties, *Food Chemistry 194* (2016) 1266-1274.

[47] S. Jafarzadeh, S. M. Jafari, Impact of metal nanoparticles on the mechanical, barrier, optical and thermal properties of biodegradable food packaging materials, *Critical reviews in food science and nutrition* (2020) 1-19.

Table captions

Table 1. WVP and WVTR results of the plasticized starch nanocomposites.

Table 2. Mechanical attributes of plasticized starch nanocomposites.

Table 3. Storage modulus (E') and glass transition temperature (T_g) (from the top peak of tan δ curve) values of the produced PS-CNPs composites**.**

Table 4a-d. The colony forming count of a) PS-1CNPs, b) PS-2CNPs, c) PS-3CNPs and d) PS-4CNPs films against *Escherichia coli* and *Staphylococcus aureus*

Tables

Table 1. WVP and WVTR results of the plasticized starch nanocomposites.

Samples	WVP ($g.m^{-1}\ s^{-1}\ Pa^{-1}$)	WVTR ($g.m^{-2}.h^{-1}$)
PS	$2.10\times10^{-7}\pm0.06\times10^{-7}$ [a]	31.97 ± 0.92 [a]
PS-1CNPs	$2.05\times10^{-7}\pm0.04\times10^{-7}$ [a]	30.27 ± 0.71 [a]
PS-2CNPs	$1.90\times10^{-7}\pm0.05\times10^{-7}$ [b]	28.04 ± 0.84 [b]
PS-3CNPs	$1.81\times10^{-7}\pm0.03\times10^{-7}$ [c]	27.22 ± 1.02 [b]
PS-4CNPs	$1.69\times10^{-7}\pm0.05\times10^{-7}$ [d]	25.03 ± 0.69 [c]

Table 2. Mechanical attributes of plasticized starch nanocomposites.

Samples	EAB (%)	TS (MPa)	E (MPa)
PS	51.01±1.32[a]	9.54±0.84[d]	16.50±1.10[e]
PS-1CNPs	46.19±1.71[b]	14.74±1.67[c]	24.20±1.04[d]
PS-2CNPs	42.10±0.98[c]	18.27±1.26[b]	29.14±1.30[c]
PS-3CNPs	39.52±1.24[d]	20.82±1.33[b]	36.12±1.45[b]
PS-4CNPs	34.29±1.69[e]	24.91±0.81[a]	47.11±2.51[a]

Table 3. Storage modulus (E') and glass transition temperature (T_g) (from the top peak of tan δ curve) values of the produced PS-CNPs composites**.**

Samples	E' (25 °C) (MPa)	E' (70 °C) (MPa)	T_g (° C)
PS	462 ± 42^{d}	90 ± 5^{d}	46 ± 2^{c}
PS-1CNPs	1258 ± 81^{c}	197 ± 9^{c}	77 ± 6^{b}
PS-2CNPs	1520 ± 69^{b}	310 ± 19^{b}	83 ± 5^{b}
PS-3CNPs	1740 ± 77^{a}	495 ± 22^{a}	101 ± 11^{a}
PS-4CNPs	1810 ± 82^{a}	510 ± 38^{a}	103 ± 8^{a}

Table 4a-d. The colony forming count of a) PS-1CNPs, b) PS-2CNPs, c) PS-3CNPs and d) PS-4CNPs films against *Escherichia coli* and *Staphylococcus aureus*.

a	Contact time	*Escherichia coli*		*Staphylococcus aureus*	
		PS-1CNPs	PS	PS-1CNPs	PS
	0 h	1.92×10^{7}	1.92×10^{7}	1.48×10^{9}	1.48×10^{9}
	24 h	8.8×10^{6}	2.38×10^{7}	0	2×10^{9}
	Increase or decrease percentage	53.16% decrease	23.95% increase	100% decrease	35.13% increase
b	Contact time	*Escherichia coli*		*Staphylococcus aureus*	
		PS-2CNPs	PS	PS-2CNPs	PS
	0 h	1.92×10^{7}	1.92×10^{7}	1.48×10^{9}	1.48×10^{9}
	24 h	5.8×10^{6}	2.38×10^{7}	0	2×10^{9}
	Increase or decrease percentage	68.02% decrease	23.95% increase	100% decrease	35.13% increase
c	Contact time	*Escherichia coli*		*Staphylococcus aureus*	
		PS-3CNPs	PS	PS-3CNPs	PS
	0 h	1.92×10^{7}	1.92×10^{7}	1.48×10^{9}	1.48×10^{9}
	24 h	4.3×10^{6}	2.38×10^{7}	0	2×10^{9}
	Increase or decrease percentage	77.60% decrease	23.95% increase	100% decrease	35.13% increase
d	Contact time	*Escherichia coli*		*Staphylococcus aureus*	
		PS-4CNPs	PS	PS-4CNPs	PS
	0 h	1.92×10^{7}	1.92×10^{7}	1.48×10^{9}	1.48×10^{9}
	24 h	3.5×10^{6}	2.38×10^{7}	0	2×10^{9}
	Increase or decrease percentage	81.77% decrease	23.95% increase	100% decrease	35.13% increase

Figure captions

Fig. 1. Topography (a) and size distribution (b) of the synthesized CNPs

Fig. 2. Water absorption capacity of plasticized starch and the resulted nanocomposites containing various concentrations of CNPs

Fig. 3. a) Storage modulus (E') and b) tan δ as a function of the temperature of the produced composites

Fig. 4. a) The weight loss and process of degradation regarding elapsed time, and, b) the visual observation of PS-CNPs composites after exposure to the white rot fungi

Fig. 5. SEM micrographs of the PS, PS-1CNPs, PS-2CNPs, PS-3CNPs, and PS-4CNPs films before (A, B, C, D, and E, respectively) and after white rot fungi degradation (a, b, c, d, and e, respectively).

Fig. 6. Disk diffusion test for *Escherichia coli* in the case of the PS-1CNPs, PS-2CNPs, PS-3CNPs, and PS-4CNPs composites, compared to neat PS (a, b, c, and d respectively).

Fig. 7. Disk diffusion test for *Staphylococcus aureus* of the PS-1CNPs, PS-2CNPs, PS-3CNPs, and PS-4CNPs composites, compared to neat PS (a, b, c, and d respectively).

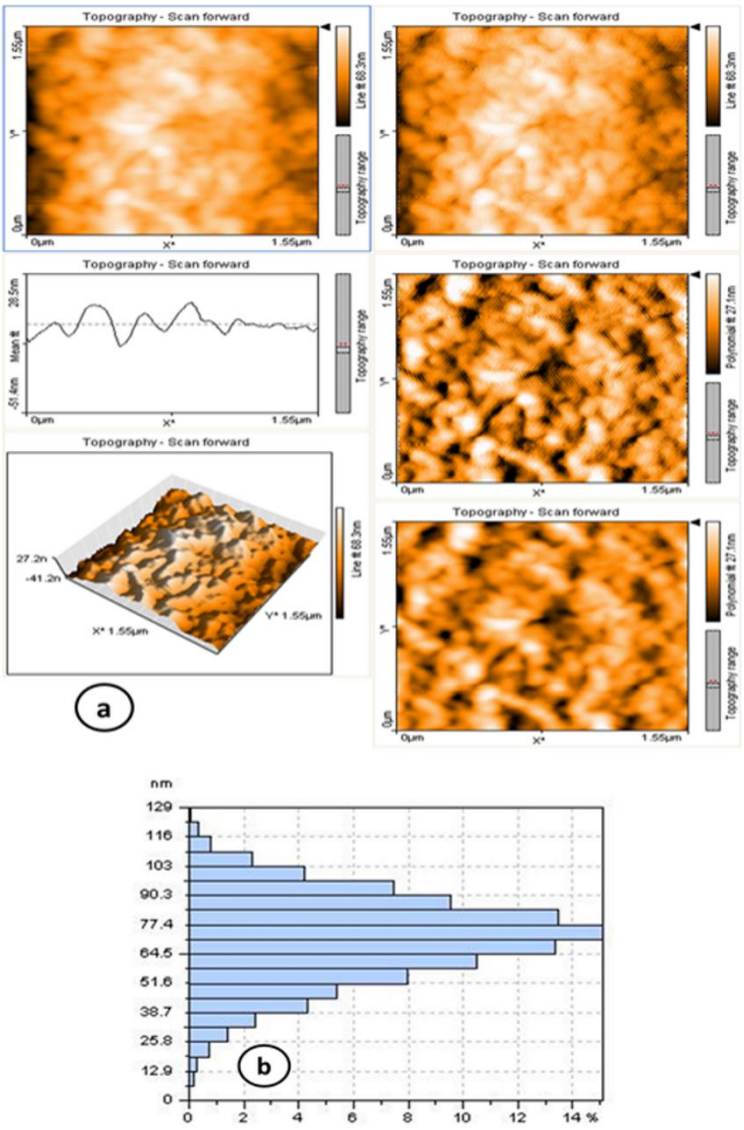
Topography - Scan forward
Topography - Scan forward
Topography - Scan forward
Topography - Scan forward
Topography - Scan forward
Topography - Scan forward
a
nm
129
116
103
90.3
77.4
64.5
51.6
38.7
25.8
12.9
0
0
2
4
6
8
10
12
14 %
b

Figure 1

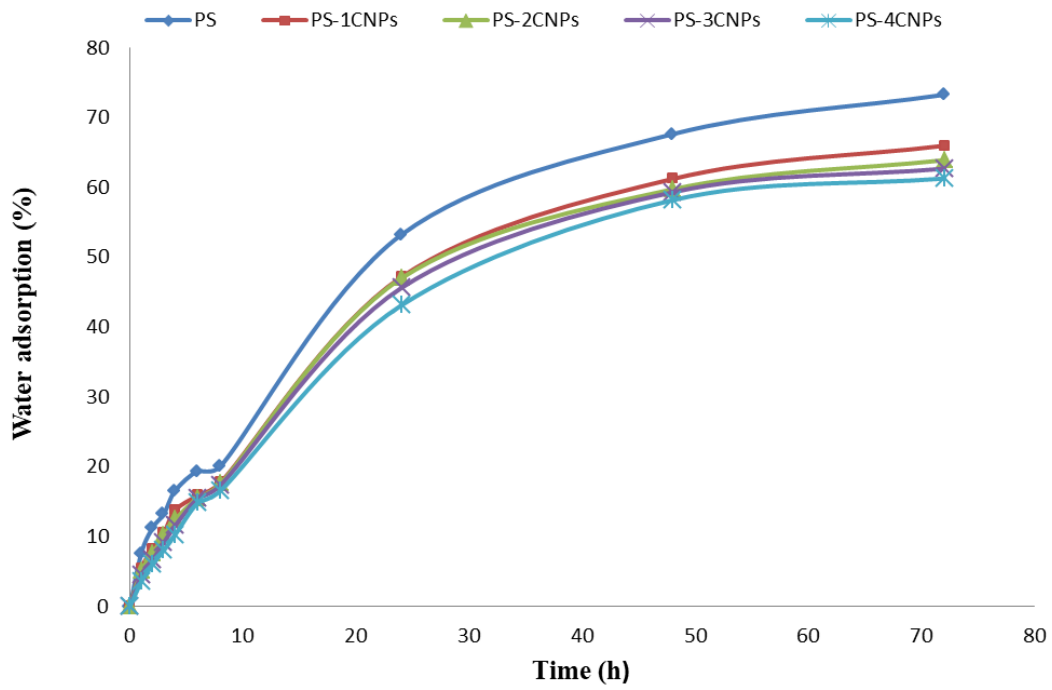
PS
PS-1CNPs
PS-2CNPs
PS-3CNPs
PS-4CNPs
Water adsorption (%)
Time (h)
0
10
20
30
40
50
60
70
80

Figure 2

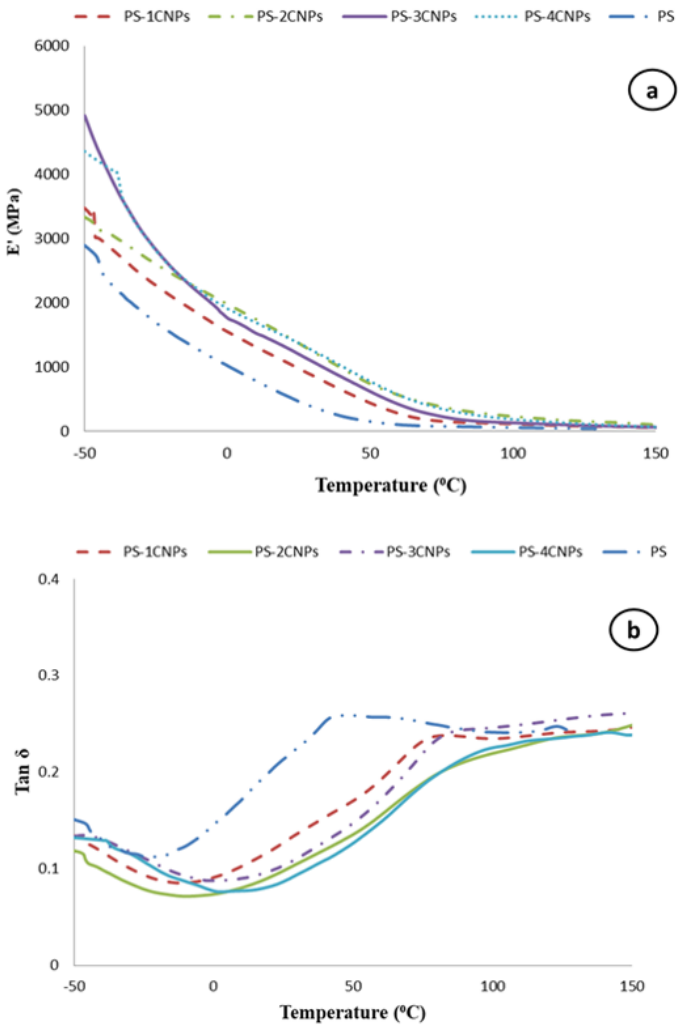
PS-1CNPs
PS-2CNPs
PS-3CNPs
PS-4CNPs
PS
a
E' (MPa)
6000
5000
4000
3000
2000
1000
0
-50
0
50
100
150
Temperature (ºC)
PS-1CNPs
PS-2CNPs
PS-3CNPs
PS-4CNPs
PS
b
Tan δ
0.4
0.3
0.2
0.1
0
-50
0
50
100
150
Temperature (ºC)

Figure 3

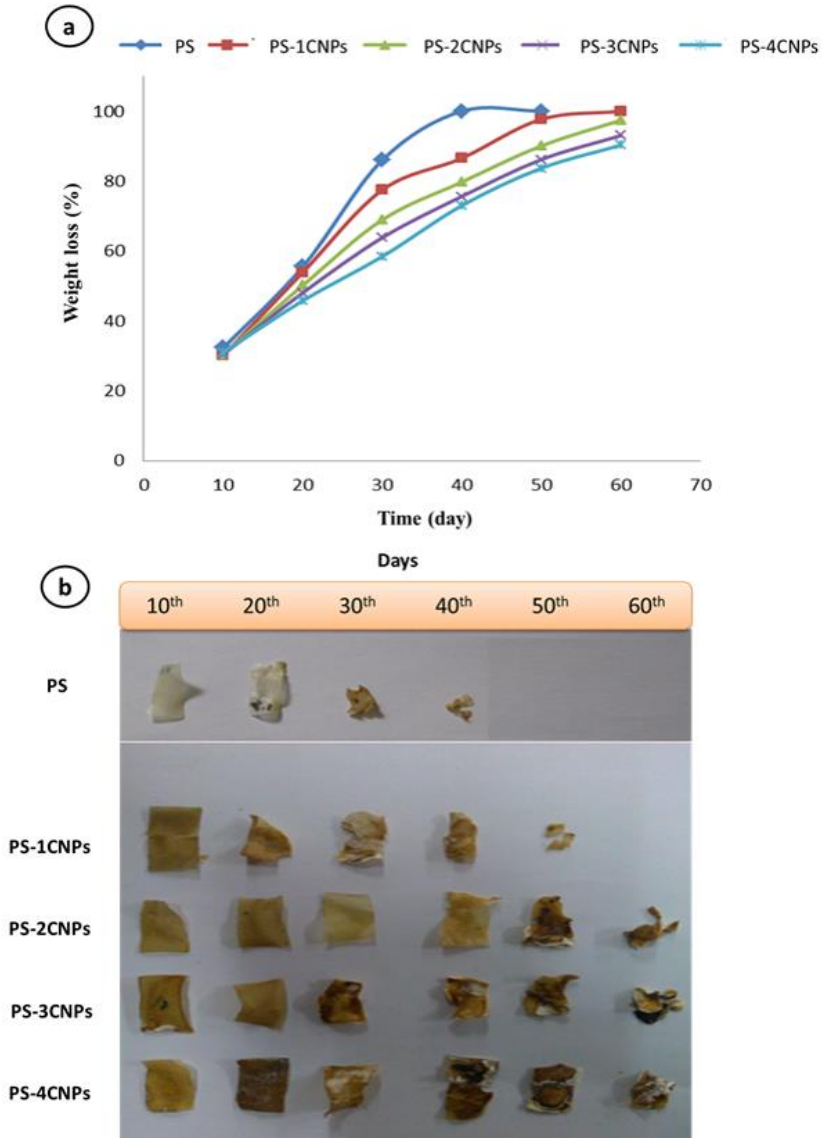
a
PS
PS-1CNPs
PS-2CNPs
PS-3CNPs
PS-4CNPs
Weight loss (%)
100
80
60
40
20
0
0
10
20
30
40
50
60
70
Time (day)
Days
b
10th
20th
30th
40th
50th
60th
PS
PS-1CNPs
PS-2CNPs
PS-3CNPs
PS-4CNPs

Figure 4

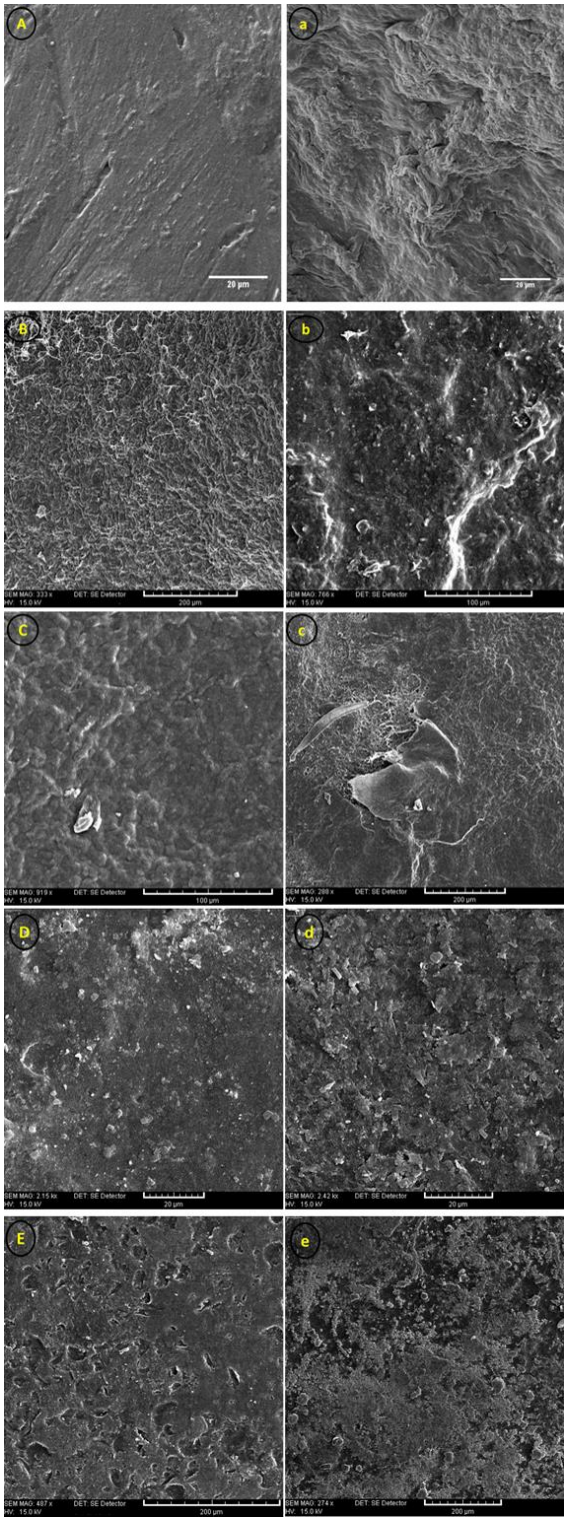

Figure 5

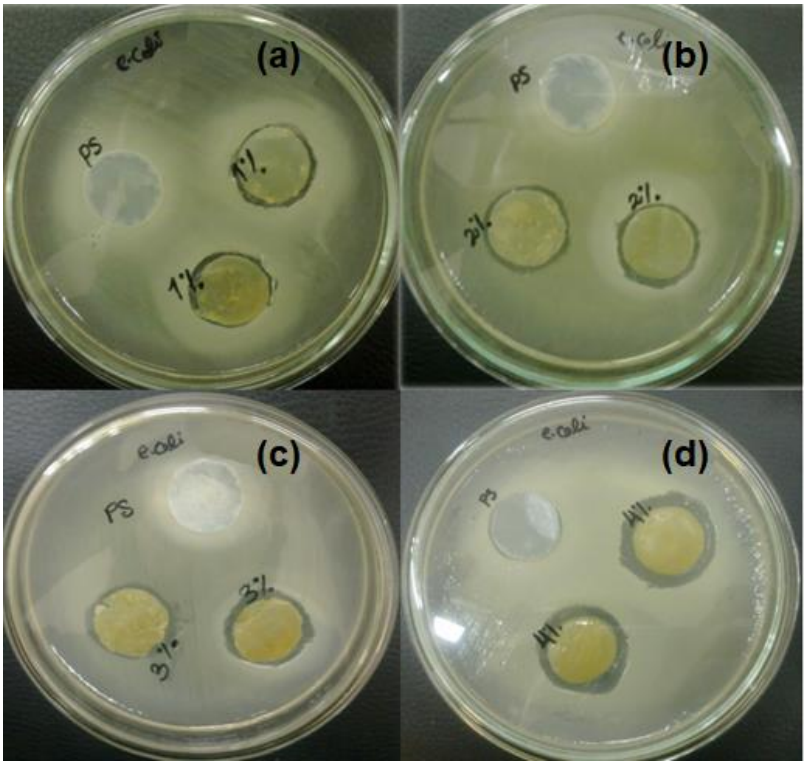

Figure 6

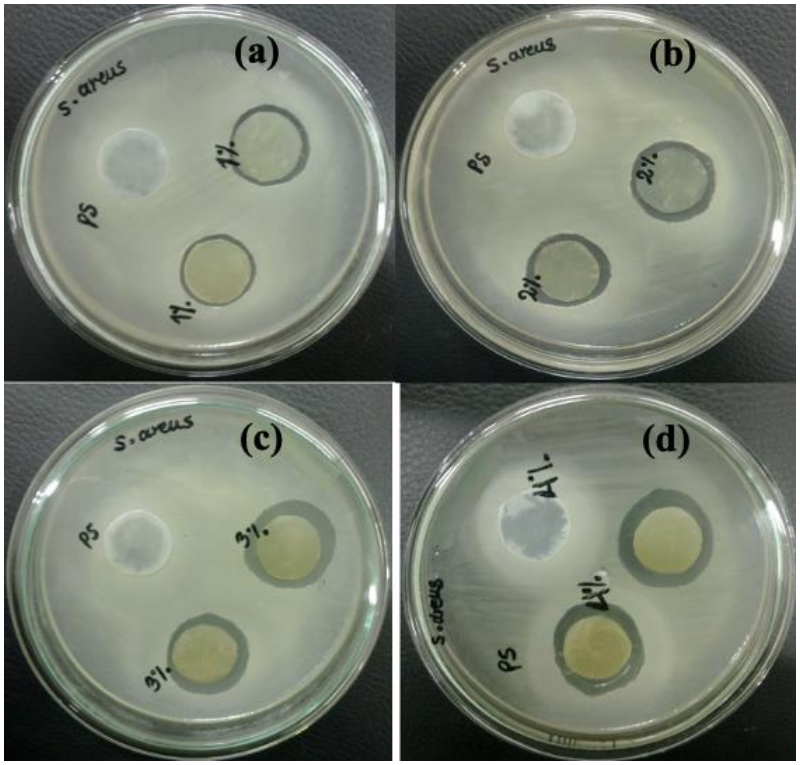

Figure 7

Samples	EAB (%)	TS (MPa)	E (MPa)	WVP ($g.m^{-1} s^{-1} Pa^{-1}$)	WVTR ($g.m^{-2}.h^{-1}$)
PS	51.01±1.32^{a}	9.54±0.84^{d}	16.50±1.10^{e}	$2.10\times10^{-7}\pm0.06\times10^{-7}$ ^{a}	31.97±0.92 ^{a}
PS-1CNPs	46.19±1.71^{b}	14.74±1.67^{c}	24.20±1.04^{d}	$2.05\times10^{-7}\pm0.04\times10^{-7}$ ^{a}	30.27±0.71 ^{a}
PS-2CNPs	42.10±0.98^{c}	18.27±1.26^{b}	29.14±1.30^{c}	$1.90\times10^{-7}\pm0.05\times10^{-7}$ ^{b}	28.04±0.84 ^{b}
PS-3CNPs	39.52±1.24^{d}	20.82±1.33^{b}	36.12±1.45^{b}	$1.81\times10^{-7}\pm0.03\times10^{-7}$ ^{c}	27.22±1.02 ^{b}
PS-4CNPs	34.29±1.69^{e}	24.91±0.81^{a}	47.11±2.51^{a}	$1.69\times10^{-7}\pm0.05\times10^{-7}$ ^{d}	25.03±0.69 ^{c}

Improvement of the mechanical and barrier properties

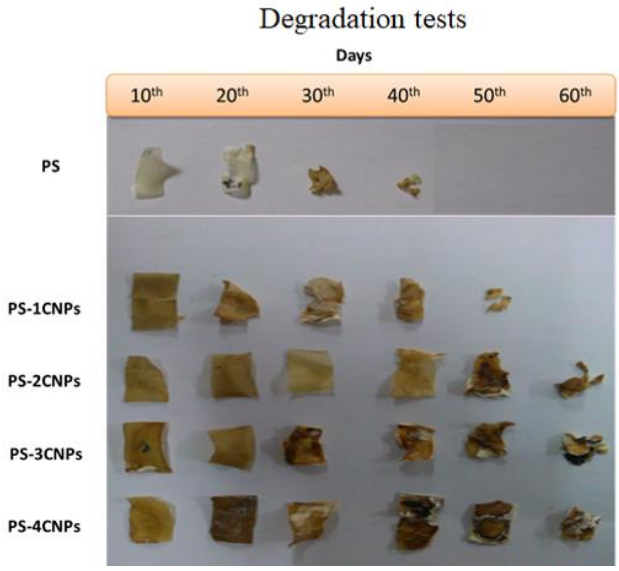

Antimicrobial action against *E. coli* and *S. aureus*

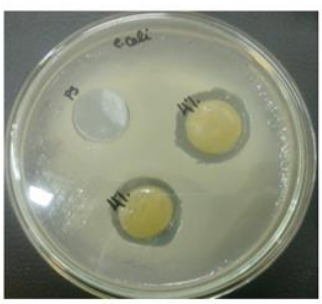

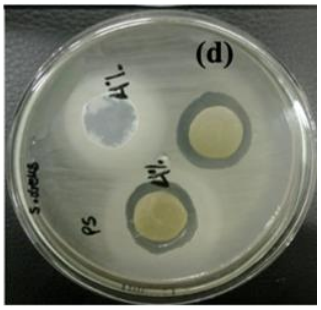

Graphical Abstract